Multistage Block-Spreading for Impulse Radio Multiple Access Through ISI Channels

Liuqing Yang, *Student Member, IEEE* and Georgios B. Giannakis, *Fellow, IEEE*

***Abstract*—Transmitting digital information using ultra-short pulses, impulse radio (IR) has received increasing interest for multiple access (MA). When IRMA systems have to operate in dense multipath environments, the multiple user interference (MUI) and intersymbol interference (ISI) induced, adversely affect system capacity and performance. Analog IRMA utilizes pulse position modulation (PPM) and random time-hopping codes to mitigate ISI and suppress MUI statistically. We develop an all-digital IRMA scheme that relies on multistage block-spreading (MS-BS), and judiciously designed transceiver pairs to eliminate MUI deterministically, and regardless of ISI multipath effects. Our proposed MS-BS-IRMA system can accommodate a large number of users and is capable of providing different users with variable transmission rates, which is important for multimedia applications. Unlike conventional IRMA systems, MS-BS-IRMA exhibits no degradation in bit-error rate performance, as the number of users increases.**

***Index Terms*—Block-spreading (BS), impulse radio (IR), multiple access (MA), multipath fading channels, time-hopping (TH), ultra-wideband (UWB) systems, wireless cellular systems.**

I. Introduction

IMPULSE RADIO (IR) or ultra-wideband (UWB) communication systems receive increasing attention thanks to their attractive features for baseband MA, low-power consumption, convenience to overlay existing infrastructure, and multimedia services. An impulse radio (IR) transmission consists of a pseudorandomly shifted train of very short pulses, where the information is encoded in their shift via pulse position modulation (PPM) [17]. The random shifts together with the ultra-short pulse shaper, and the data modulation result in a transmitted signal with low power spectral density spread across the ultra-wide bandwidth.

IR technology equipped with time-hopping (TH) codes was proposed in [10] and [17], where it is referred to as impulse radio multiple access (IRMA). Subsequent works have focused on optimizing the efficiency of IRMA by characterizing the channel, improving the modulation format, and addressing networking aspects; see [3], [7], [8], [14], [16], and references therein.

IRMA systems have to operate often in dense multipath environments. Based on experimental measurements, it was shown in [15] that IR signalling provides resolvable multipath components and enables collecting energy from multipath propagation with appropriate receiver designs (see e.g., [13]). This is true provided that the observation window is long enough, and intersymbol interference (ISI) is avoided by adjusting system parameters. However, when multiple users present, the multipath propagation also induces multiuser interference (MUI). The MUI, together with ISI, affects system capacity and performance severely [1], [4]. In the analog IRMA schemes proposed so far, the MUI is treated as Gaussian noise, and it is suppressed only statistically. Such schemes require successful application of (strict) power control and rely on the Gaussian approximation of the MUI [7], [16]. However, when the number of users is not large enough, the Gaussian approximation is not valid. On the other hand, as the number of users increases, bit-error rate (BER) performance degrades with fixed power, while additional power becomes a must for a given BER [16]. The single-user case has been tested in [1], [4], [8], but the performance of analog IRMA transmissions over ISI multipath channels has not been studied thoroughly. Recently, a digital IRMA model was developed in [5], [6]. This scheme is tailored to a *downlink* scenario, and invokes multiuser detection (MUD) to improve upon the statistical MUI cancellation. However, [5], [6] is not suitable for the uplink operation; but even in the downlink, the receiver designs require inversion of large size matrices. In addition, the maximum number of users the system can accommodate is quite limited compared to the conventional IRMA system [16].

In this paper, we develop an all-digital IR that relies on multistage block-spreading (MS-BS) operations to gain resilience to MUI and ISI. Chip-interleaved block-spread code-division multiple access (CIBS-CDMA) was developed in [18] to eliminate MUI *deterministically* at the receiver by parsing the information stream into blocks, on which block-spreading, and chip interleaving is applied before transmission. CIBS-CDMA relies on linear modulation, and is suitable for a bandwidth-efficient setup. Here, we show that in power-efficient IRMA systems using orthogonal M-ary PPM modulation, the features of CIBS in MUI elimination still hold when the transceivers are designed based on our novel MS-BS operations. Those render the MA channel equivalent to a set of independent parallel single-user frequency-selective channels with additive white Gaussian noise (AWGN), on which any single-user equalizer can be employed. Our transceivers, that we naturally term multistage block-spread IRMA (MS-BS-IRMA), have low-complexity, and are applicable to both *uplink* and *downlink* setups. Furthermore, thanks to the two stages of block-spreading, the proposed system can accommodate a large number of users, and is capable of providing different users with variable transmission rates, which is important for certain

Manuscript received January 10, 2002; revised July 30, 2002. This work was supported in part by the ARL/CTA under Grant DAAD19-01-2-011, and in part by a DARPA subcontract from General Dynamics. This paper was presented in part at the IEEE Conference on Ultra-Wideband Systems and Technologies, Baltimore, MD, May 20–23, 2002.

The authors are with the Department of Electrical and Computer Engineering, University of Minnesota, Minneapolis, MN 55455 USA (e-mail: lqyang@ece.umn.edu; georgios@ece.umn.edu).

Digital Object Identifier 10.1109/JSAC.2002.805621

multimedia applications. As the number of users increases, MS-BS-IRMA shows no degradation in BER performance, in contrast to what can be observed in conventional IRMA systems.

In Section II, we develop a digital M-ary PPM-IRMA model starting from the conventional continuous-time model described in [14]. The multipath channel is also introduced in this section, along with the digital equivalent channel model. Based on the signal and channel models, the MS-BS-IRMA schemes together with the system model in matrix-vector form, are derived in Section III. Our digital transceiver designs developed in Section IV are based on a specific BS operation, which similar to [18], can be viewed as (and is implemented by) symbol-spreading followed by chip-interleaving. Thanks to chip interleaving and zero-padding at the transmitter, mutual orthogonality between different users' addresses is preserved even after multipath propagation, which enables deterministic multiuser separation. Consequently, MUD is successfully converted to a set of equivalent single user equalization problems. Discussion of several features of the proposed system is presented in Section IV. Simulations are performed in Section V, where comparisons and performance analysis are shown. Finally, conclusions are given in Section VI.

Notation: Bold upper (lower) letters denote matrices (column vectors); $(\cdot)^T$ and $(\cdot)^{\mathcal{H}}$ denote transpose and Hermitian transpose, respectively; $\delta(\cdot)$ and $\otimes$ stand for Kronecker's delta and Kronecker product, respectively. $E\{\cdot\}$ for expectation, $\lfloor\cdot\rfloor$ for integer floor, and $\lceil\cdot\rceil$ for integer ceiling; $\boldsymbol{I}_K$ denotes the identity matrix of size K; and $\mathbf{0}_{M\times N}$ denotes an all-zero matrix with size $M\times N$.

II. M-ARY PPM-IRMA MODELING

In this section, we develop a digital M-ary PPM-IRMA model starting from the conventional continuous-time model [14]. We also introduce the multipath model and present the discrete-time equivalent channel model.

A. Signal Model With TH

To facilitate the transition from the continuous-time PPM to our BS model, we first briefly review the PPM-IRMA setup in the single-user case, and its links with the linearly modulated CDMA model in [5] and [6].

In M-ary PPM-IRMA, for each, e.g., the uth user, every transmitted M-ary PPM symbol is repeated over N_f frames each having duration T_f. During a signalling interval of duration $T_s = N_f T_f$ seconds, $k_b = \log_2 M$ message bits of a user, having a bit rate R_b, are loaded in a k_b-bit buffer. Hence, the k_b-bit output symbol rate is $R_s = R_b/k_b$. We denote the uth user's information bearing symbol transmitted during the kth frame as $I_u(\lfloor k/N_f\rfloor)$, where $I_u(\lfloor k/N_f\rfloor)\in[0, M-1]$.

Each frame comprises N_c chips. With T_c denoting chip duration, we have $T_f = N_c T_c + T_g$, where T_g is a guard time introduced to account for processing delay at the receiver between two successively received frames. The uth user's transmitted waveform is given by

$$\nu_u(t) = \mathcal{P}_u \sum_{k=-\infty}^{+\infty} w\left(t - kT_f - \tilde{c}_u(k)T_c - \tau_{I_u(\lfloor k/N_f\rfloor)}\right) \quad (1)$$

where $\mathcal{P}_u$ is the uth user's transmission power, $w(t)$ denotes the ultra-short monopulse, and $\tilde{c}_u(k)\in[0, N_c-1]$ is a periodic TH pseudorandom sequence with period $P_{\tilde{c}} = N_f$. The role of $\tilde{c}_u(k)$ is to enable MA, and security in e.g., military communications. Each segment of duration $N_f T_f$ contains N_f copies of a single symbol (one per frame), and the monopulse is time-shifted in each frame according to the symbol value; e.g., it is shifted by τ_m if $I_u(\lfloor k/N_f\rfloor) = m$, for $m\in[0, 1, \ldots, M-1]$. Let T_w denote the monopulse duration. In order to ensure orthogonal modulation, PPM modulation delays τ_m must satisfy $\tau_m - \tau_{m-1}\geq T_w, \forall m\in[1, 2, \ldots, M-1]$. Thus, the chip duration is chosen to satisfy: $T_c \geq \tau_{M-1} + T_w \geq MT_w$. One way to model this mapping is to have M parallel branches each realizing a shifted version of the pulse stream. In order to generate the signal $\nu_u(t)$, we then only need to select one branch (out of M) depending on the symbol value. Adopting this viewpoint, we can reexpress (1) as

$$\nu_u(t) = \sum_{m=0}^{M-1} \nu_{u,m}(t) \quad (2)$$

with

$$\nu_{u,m}(t) = \mathcal{P}_u \sum_{k=-\infty}^{+\infty} s_{u,m}(\lfloor k/N_f\rfloor) \times w(t - kT_f - \tilde{c}_u(k)T_c - \tau_m) \quad (3)$$

where $s_{u,m}(\lfloor k/N_f\rfloor) := \delta(I_u(\lfloor k/N_f\rfloor) - m), \forall m\in[0, M-1]$. Upon defining the time-shifted pulses $w_m(t) := w(t-\tau_m)$, and recalling that $T_f = N_c T_c$ for $T_g = 0$, (3) can be rewritten as

$$\nu_{u,m}(t) = \mathcal{P}_u \sum_{k=-\infty}^{+\infty} s_{u,m}(\lfloor k/N_f\rfloor) w_m(t - (kN_c + \tilde{c}_u(k))T_c). \quad (4)$$

Because $\tilde{c}_u(k)\in[0, N_c-1]$ is an integer, we infer that $w_m(t)$ in (4) is shifted by an integer multiple of T_c. It is thus possible to view $\nu_{u,m}(t)$ as a linearly modulated waveform with symbol rate $1/T_c$, and express it as

$$\nu_{u,m}(t) = \mathcal{P}_u \sum_{n=-\infty}^{+\infty} \nu_{u,m}(n) w_m(t - nT_c), \quad (5)$$

where $\nu_{u,m}(n)$ is a sequence that depends on $s_{u,m}(k)$, and $\tilde{c}_u(k)$. Equation (2) can be interpreted as the superposition of M linear modulators, each with a different pulse function $w_m(t)$.

Let us consider a new chip-rate code sequence $c_u(n)$ defined via $\tilde{c}_u(k)$ as follows:

$$c_u(n) := \delta(\lfloor n/N_c\rfloor N_c + \tilde{c}_u(\lfloor n/N_c\rfloor) - n). \quad (6)$$

It can be readily verified by direct substitution that the period of $c_u(n)$ in (6) is $P_c = N_c P_{\tilde{c}}$. An example is shown in Fig. 1 to illustrate the relation between $c_u(n)$ and $\tilde{c}_u(k)$. Clearly the two are related by a mapping between the chip index n, and the frame index k. The reason we introduced $c_u(n)$ is because the

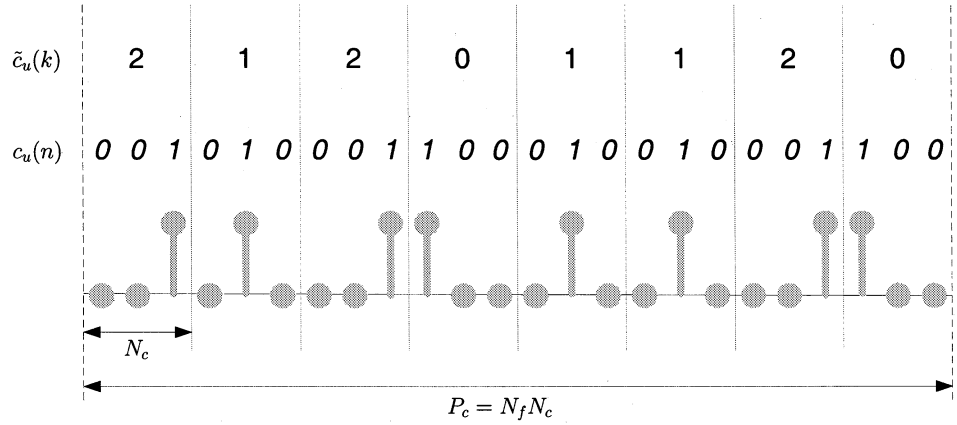

Fig. 1. Relation between $c_u(n)$ and $\tilde{c}_u(k)$. $N_c = 3$, $N_f = 8$.

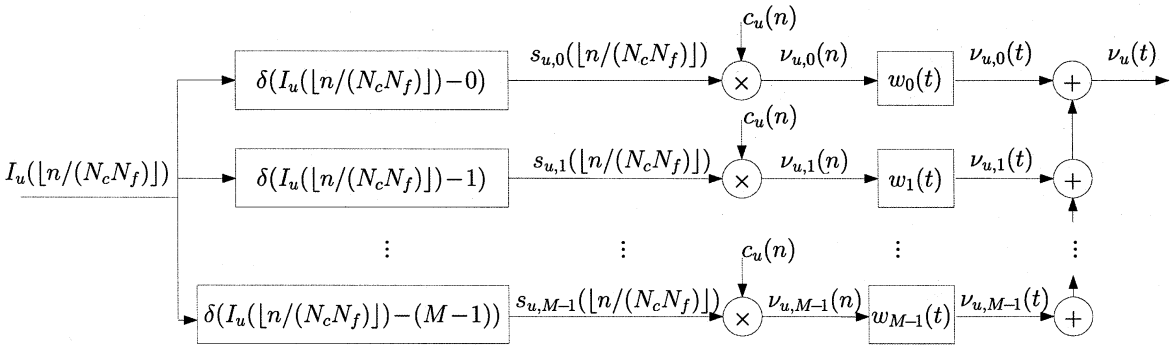

Fig. 2. TH PPM modulation of the uth user. During the nth chip duration, the transmitted symbol is $I_u(\lfloor n/(N_cN_f)\rfloor)$.

uth user's chip sequence on the mth branch $\nu_{u,m}(n)$ in (5) can be conveniently expressed as

$$\nu_{u,m}(n) = s_{u,m}(\lfloor n/(N_cN_f)\rfloor)c_u(n). \tag{7}$$

The TH PPM modulation of the uth user at the chip-rate is illustrated in Fig. 2. Notice that the information carrying stream $I_u(\lfloor n/(N_cN_f)\rfloor)$, and thus $s_{u,m}(\lfloor n/(N_cN_f)\rfloor)$, does not change over the duration of N_fT_f s (N_fN_c chips). It is spread by the TH address $c_u(n)$ to generate the chip sequence $\nu_{u,m}(n)$ in (7). From this chip-rate sampled model, the nonlinearly modulated PPM-IRMA model can be viewed as a linearly modulated CDMA system [5], [6].

We have assumed here for simplicity that $T_g = 0$, although the model can encompass $T_g \neq 0$ as well. This can be accomplished by setting $T_g = N_gT_c$ with N_g integer, and restricting the sequence $\tilde{c}_u(k)$ to take its values on $[0, N_c' - 1]$, where $N_c' := N_c - N_g$. Hereafter, we will assume $T_g = 0$.

B. Channel Model

The transmitted signal $\nu_{u,m}(t)$ propagates through a channel $g_u(t)$, and is filtered by a multibranch receiver with the filter on the m'th branch $\bar{w}_{m'}(t)$ matched to $w_{m'}(t)$, where $m' \in [0, M-1]$. With $\star$ denoting convolution, let $h_{u,m',m}(l) := (w_m \star g_u \star \bar{w}_{m'})(t)|_{t=lT_c}$ be the chip-sampled discrete time equivalent FIR channel. The FIR channel $h_{u,m',m}(l)$ of order L_u includes the uth user's asynchronism in the form of delay factors as well as transmit-receive filters, and the multipath effects. Let $\eta_{m'}(n) := (\eta \star \bar{w}_{m'})(t)|_{t=nT_c}$ denote sampled noise. The chip-sampled matched filter output of the m'th branch at the receiver is

$$x_{m'}(n) = \sum_{u=0}^{N_u-1}\sum_{m=0}^{M-1}\sum_{l=0}^{L}\mathcal{P}_u h_{u,m',m}(l)\nu_{u,m}(n-l) + \eta_{m'}(n) \tag{8}$$

where N_u is the number of users, $L := \max_u L_u$, and M is the number of PPM pulse shapers.

Here, we focus on a cellular quasi-synchronous system in the *uplink*, where the mobile users attempt to synchronize with the base-station's pilot waveform, and have a coarse common timing reference. Asynchronism among users is thus limited to only a few chip intervals; the maximum asynchronism $\tau_{\max,a}$ arises between the nearest and the farthest mobile users. With $\tau_{\max,s}$ denoting maximum multipath spread, which is found using field measurements from the operational environment, the maximum channel order can be found as $L = \lceil(\tau_{\max,s} + \tau_{\max,a})/T_c\rceil$.

The *downlink* model (from the base station to the user of interest μ) is subsumed by the uplink model (8): indeed, setting $h_{u,m',m}(l) = h_{\mu,m',m}(l), \forall u \in [0, N_u - 1]$, is a special case of (8) since the latter allows for distinct user channels. The downlink transmissions are synchronous with $\tau_{\max,a} = 0$, and the maximum channel order L depends only on $\tau_{\max,s}$ through

$L = \lceil \tau_{\max,s}/T_c \rceil$. In either uplink or downlink, the only channel knowledge assumed at the transmitter is L.

III. Digital MS-BS-IRMA Transmitter

To facilitate separation of multiple users, and thus eliminate the MUI at the receiver, we start by assigning to each user a TH address vector of length $P_{\tilde{c}} = N_f$ denoted by

$$\tilde{\boldsymbol{c}}_{u_A} := [\tilde{c}_{u_A}(0), \ldots, \tilde{c}_{u_A}(P_{\tilde{c}} - 1)]^T \tag{9}$$

with $\tilde{c}_{u_A}(n) \in [0, N_c - 1]$, and $\tilde{c}_{u_A}(n) \neq \tilde{c}_{\mu_A}(n), \forall n \in [0, P_{\tilde{c}} - 1]$ and any two users u, μ. Recalling that the total number of chips in one frame is N_c, it follows that the number of such TH address vectors can be at most N_c. If the number of active users satisfies $N_u \leq N_c$, then N_u out of the N_c TH addresses can be uniquely assigned to the N_u users. Let us now define the TH spreading codes

$$\boldsymbol{c}_{u_A} = [c_{u_A}(0), c_{u_A}(1), \ldots, c_{u_A}(P_c - 1)]^T, \quad c_{u_A}(n) \in [0, 1]$$

of length $P_c = N_c P_{\tilde{c}} = N_c N_f$, and with $c_{u_A}(n)$ defined as in (6). It can be readily shown that no collisions occur between any two users by design, since these code vectors are mutually orthogonal, i.e., $\boldsymbol{c}_{u_A}^{\mathcal{H}} \boldsymbol{c}_{\mu_A} = N_f \delta(u_A - \mu_A), \forall u_A, \mu_A \in [0, N_c - 1]$.

But what if the number of active users is $N_u > N_c$? In such cases, it is inevitable that more than one users are assigned the same TH address. Recall from Section II that identical information symbols are sent over N_f frames. This can be viewed as encoding each symbol with a repetition code. In order to distinguish between different users who share the same TH address, we can replace the repetition code with a user-signature pattern that will henceforth be referred to as multiuser (MU) address. Let the u_Bth MU address be expressed as

$$\boldsymbol{d}_{u_B} := [d_{u_B}(0), \ldots, d_{u_B}(N_f - 1)]^T, \qquad d_{u_B}(n) \in [1, -1] \tag{10}$$

and suppose it is designed to satisfy $\boldsymbol{d}_{u_B}^{\mathcal{H}} \boldsymbol{d}_{\mu_B} = N_f \delta(u_B - \mu_B), \forall u_B, \mu_B \in [0, N_f - 1]$. The repetition encoding of Section II can be realized by simply setting $\boldsymbol{d}_{u_B} = [1, 1, \ldots, 1]^T, \forall u_B$.

If the number of users N_u satisfies $N_u \leq N_c N_f$, then a given TH address has to be assigned to $\lfloor N_u/N_c \rfloor$ or $\lceil N_u/N_c \rceil$ users, which form a user group. In order to be able to resolve users in the same group, we assign an additional set of MU addresses by employing a unique mapping to each of the $\lfloor N_u/N_c \rfloor$ or $\lceil N_u/N_c \rceil$ users in the same group, in order to distinguish them from each other. Note that the same MU address can be assigned to several users that belong to different groups, since the groups are differentiated via their unique TH addresses. Systematically, we assign the TH and MU addresses to each user, e.g., the uth user ($u \in [0, N_c N_f - 1]$), as follows.

1) Assign to the uth user the TH address with index $u_A = u (\mathrm{mod} N_c)$;.

2) Assign to the uth user the MU address with index $u_B = \lfloor u/N_c \rfloor$.

As illustrated by the example in Fig. 3 for $N_u = 32$, indices of users are loaded in a matrix having $N_c = 4$ rows and $N_f = 8$ columns. Each two-dimensional (2-D) coordinate (matrix entry) determines the MU and TH addresses of a specific user. It is evident that given a user u, its $\{u_A, u_B\}$ pair is uniquely determined and vice versa. Therefore, if the number of users $N_u \leq N_c N_f$, the probability of hits or collisions is zero. Hereafter, we consider the fully loaded system, where the number of users $N_u = N_f N_c$.

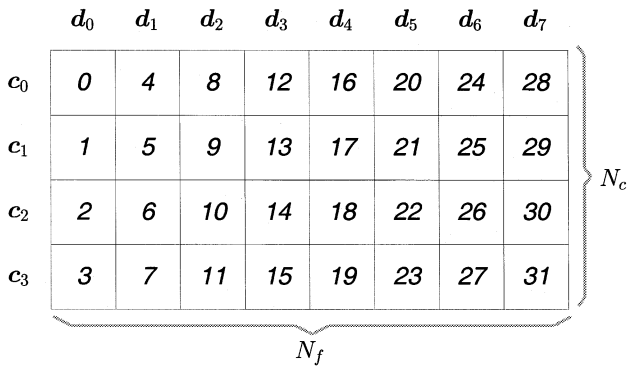

Fig. 3. MU and TH address assignment example. $N_f = 8$, $N_c = 4$, $N_u = 32$.

As mentioned earlier, corresponding to each user signature address we assign a unique user spreading code. Based on our multistage user signature spreading code assignment, we are going to introduce user-specific block-spreading codes, and design the corresponding MS-BS scheme, which will be shown capable of separating multiple users, and eliminating the MUI deterministically at the receiver, regardless of the underlying frequency-selective channels.

A. MU Block-Spreading Stage

The nth transmitted symbol on the mth branch of user u, that we denoted as $s_{u,m}(n)$, is signalled by invoking the uth user's MU address, and can be expressed as

$$\tilde{s}_{u,m}(n) := s_{u,m}(\lfloor n/N_f \rfloor) d_{u_B}(n). \tag{11}$$

As we saw in Section II-A, the TH-IRMA model can be viewed as a CDMA system, where each symbol is spread according to the user's TH address. We can view the spreading with MU addresses in the same manner. Notwithstanding, unlike traditional spreading that is performed over a *single symbol*, we here use block spreading that operates on a *block of symbols*. Specifically, the information stream on the mth branch of the uth user $s_{u,m}$ is first parsed into blocks of length K

$$\boldsymbol{s}_{u,m}(i) := [s_{u,m}(iK), \ldots, s_{u,m}(iK + K - 1)]^T$$

and then block-spread by a user-specific $Q \times K$ spreading matrix $\boldsymbol{D}_{u_B}$ to obtain the $Q \times 1$ output vector $\tilde{\boldsymbol{s}}_{u,m}(i) = \boldsymbol{D}_{u_B} \boldsymbol{s}_{u,m}(i)$, where $\tilde{\boldsymbol{s}}_{u,m}(i) := [\tilde{s}_{u,m}(iQ), \ldots, \tilde{s}_{u,m}(iQ + Q - 1)]^T$. Viewing each column of $\boldsymbol{D}_{u_B}$ (with the $(k+1)$st column denoted by $\boldsymbol{d}_{u_B}^{(k)}$) as a separate spreading code for user u, the block spreading operation implements a multicode transmitter (K codes per user) [11]. Indeed, we can write the transmitted block as: $\tilde{\boldsymbol{s}}_{u,m}(i) = \sum_{k=0}^{K-1} s_{u,m}(iK + k) \boldsymbol{d}_{u_B}^{(k)}$.

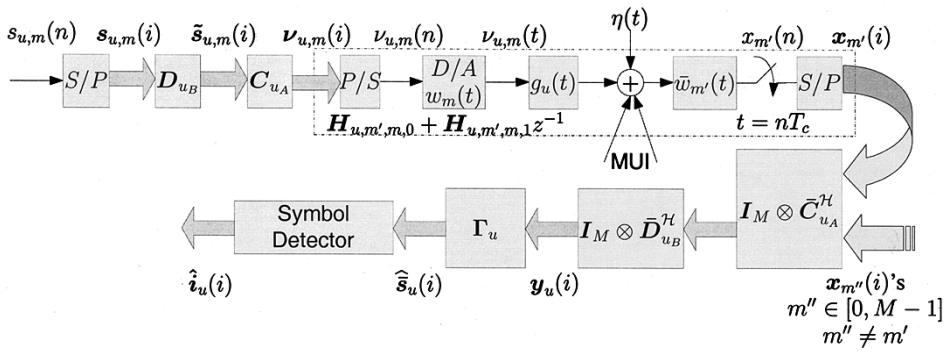

Fig. 4. Continuous and discrete-time equivalent system model of the uth user (only the mth branch at the transmitter and the m'th branch at the receiver are shown).

B. TH Block-Spreading Stage

Similar to the MU address BS, we introduce the TH spreading matrix $\boldsymbol{C}_{u_A}$ for the uth user; and use it to recast (7) in a matrix-vector form $\boldsymbol{\nu}_{u,m}(i) = \boldsymbol{C}_{u_A}\tilde{\boldsymbol{s}}_{u,m}(i)$, where the $P \times 1$ vector on the mth branch is $\boldsymbol{\nu}_{u,m}(i) := [\nu_{u,m}(iP), \ldots, \nu_{u,m}(iP+P-1)]^T$. We will later on specify the $P \times Q$ TH address matrix $\boldsymbol{C}_{u_A}$ and the corresponding receiver matrix, which guarantee the MUI elimination by design.

Notice that the MU BS is performed at the frame-level, i.e., a block of K symbols are spread into Q frame-rate signals (each of duration T_f); whereas the TH BS is performed at the chip-level, i.e., the block of Q frame-rate signals are further spread into P chip-rate signals (each of duration T_c) by the TH spreading matrices $\boldsymbol{C}_{u_A}$.

C. Multistage Matrix-Vector Model

The block diagram in Fig. 4 describes our MS-BS IRMA model in either *uplink* or *downlink* operation, where only one branch of the uth user is shown. As the output of the two-stage BS module, the signal block to be transmitted on the mth branch of the uth user is given by

$$\boldsymbol{\nu}_{u,m}(i) = \boldsymbol{C}_{u_A}\boldsymbol{D}_{u_B}\boldsymbol{s}_{u,m}(i) \tag{12}$$

where u_A and u_B are indices of the TH and MU addresses assigned to the uth user, respectively. As shown in Fig. 4, $\boldsymbol{\nu}_{u,m}(i)$ is first parallel to serial (P/S) converted; it then propagates through the equivalent channel, which accounts for the mth pulse shaper, the corresponding physical channel and the m'th matched filter. Upon reception, noise and MUI are added, to yield the received chip-rate sampled sequence

$$x_{m'}(n) = \sum_{u=0}^{N_u-1}\sum_{m=0}^{M-1}\sum_{l=0}^{L}\mathcal{P}_u h_{u,m',m}(l)\nu_{u,m}(n-l) + \eta_{m'}(n).$$

At the receiver, $x_{m'}(n)$ samples are serial to parallel (S/P) converted to form $P \times 1$ blocks

$$\boldsymbol{x}_{m'}(i) := [x_{m'}(iP), x_{m'}(iP+1), \ldots, x_{m'}(iP+P-1)]^T$$

which are observed in the presence of noise blocks

$$\boldsymbol{\eta}_{m'}(i) := [\eta_{m'}(iP), \eta_{m'}(iP+1), \ldots, \eta_{m'}(iP+P-1)]^T.$$

Let $\boldsymbol{H}_{u,m',m,0}$ be the $P \times P$ lower triangular Toeplitz matrix with first column $[h_{u,m',m}(0), \ldots, h_{u,m',m}(L), 0, \ldots, 0]^T$, and $\boldsymbol{H}_{u,m',m,1}$ be the $P \times P$ upper triangular Toeplitz matrix with first row $[0, \ldots, 0, h_{u,m',m}(L), \ldots, h_{u,m',m}(1)]$. The input–output block relationship of our system can be described in matrix-vector form as

$$\boldsymbol{x}_{m'}(i) = \sum_{u=0}^{N_u-1}\sum_{m=0}^{M-1}\mathcal{P}_u[\boldsymbol{H}_{u,m',m,0}\boldsymbol{\nu}_{u,m}(i) + \boldsymbol{H}_{u,m',m,1}\boldsymbol{\nu}_{u,m}(i-1)] + \boldsymbol{\eta}_{m'}(i) \tag{13}$$

where $\boldsymbol{\nu}_{u,m}(i)$ is defined in (12). Making use of the address assigning rules and (12), we can reexpress (13) as

$$\boldsymbol{x}_{m'}(i) = \sum_{u_A=0}^{N_c-1}\sum_{u_B=0}^{N_f-1}\sum_{m=0}^{M-1}\mathcal{P}_u[\boldsymbol{H}_{u,m',m,0}\boldsymbol{C}_{u_A}\boldsymbol{D}_{u_B}\boldsymbol{s}_{u,m}(i) + \boldsymbol{H}_{u,m',m,1}\boldsymbol{C}_{u_A}\boldsymbol{D}_{u_B}\boldsymbol{s}_{u,m}(i-1)] + \boldsymbol{\eta}_{m'}(i). \tag{14}$$

Notice that the $\boldsymbol{s}_{u,m}(i-1)$ dependent term in (14) accounts for the so-called interblock interference (IBI).

IV. Digital MS-BS-IRMA Receiver

We describe here our digital IRMA design that relies on MS-BS. The latter is described by (12), and can be implemented efficiently by symbol-spreading followed by chip-interleaving as detailed in [18]. The resulting MS-BS based MUI-free transceivers are applicable to both *downlink* and *uplink* operations. Since PPM is a nonlinear modulation, the receivers will operate in three stages: 1) a linear filtering stage to separate multiple users and, thus, render the multiple-access channel equivalent to a set of single-user ISI channels; 2) a stage employing single-user channel equalizers to eliminate channel effects; and 3) a symbol detection stage.

The first stage of the receiver employs a multiuser separating front-end, which is described by the despreading matrices $\bar{\boldsymbol{C}}_{\mu_A}$ and $\bar{\boldsymbol{D}}_{\mu_M}$ for the μth user. The goal of this stage is to extract the μth user's signal from $\boldsymbol{x}_{m'}(i)$, and yield the MUI-free block

$$\boldsymbol{y}_{\mu,m'}(i) = \bar{\boldsymbol{D}}^{\mathcal{H}}_{\mu_B}\bar{\boldsymbol{C}}^{\mathcal{H}}_{\mu_A}\boldsymbol{x}_{m'}(i), \quad \forall m' \in [0, M-1]. \tag{15}$$

At the second stage, the MUI-free output $\boldsymbol{y}_\mu(i) := [\boldsymbol{y}^T_{\mu,0}(i), \boldsymbol{y}^T_{\mu,1}(i), \ldots, \boldsymbol{y}^T_{\mu,M-1}(i)]^T$ can then be equalized by *any* single

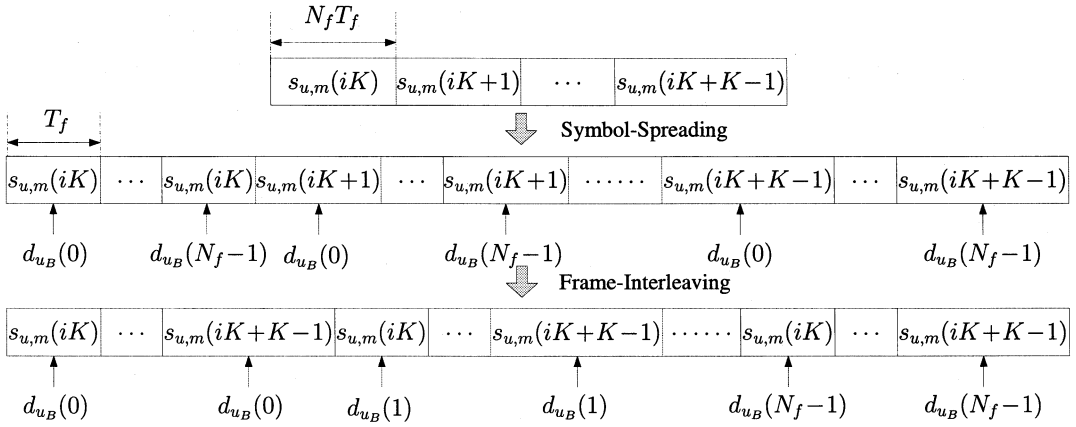

Fig. 5. MU BS stage with MU address matrices $\boldsymbol{D}_{u_B}$ in (17).

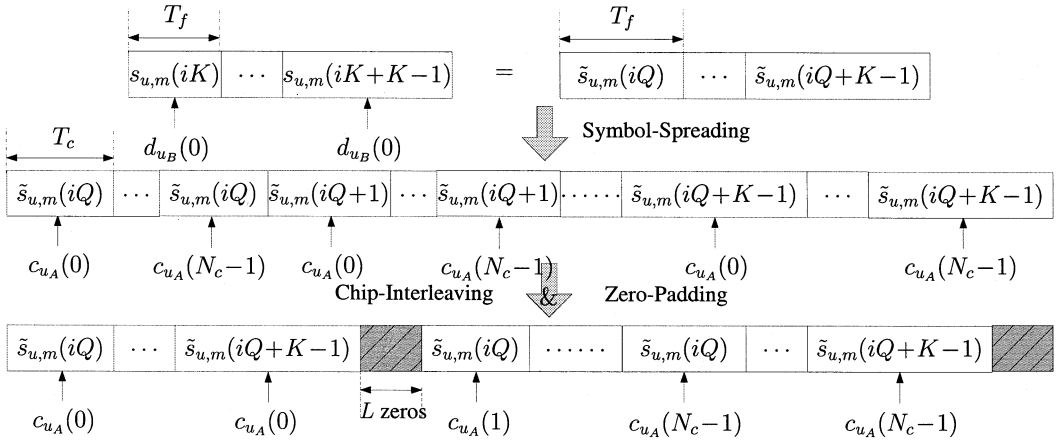

Fig. 6. TH spreading of a subblock with TH address submatrix $\boldsymbol{C}_{u_A}^{(0)}$.

user equalizer; e.g., a linear equalizer $\boldsymbol{\Gamma}_\mu$ will yield symbol block estimates

$$\hat{\tilde{\boldsymbol{s}}}_\mu(i) = \boldsymbol{\Gamma}_\mu \boldsymbol{y}_\mu(i) \tag{16}$$

where $\hat{\tilde{\boldsymbol{s}}}_\mu(i) := [\hat{\boldsymbol{s}}_{\mu,0}^T(i), \hat{\boldsymbol{s}}_{\mu,1}^T(i), \ldots, \hat{\boldsymbol{s}}_{\mu,M-1}^T(i)]^T$.

Finally, symbol detection is performed based on the soft estimates $\hat{\tilde{\boldsymbol{s}}}_\mu(i)$.

Starting from the general block-spread transmission model developed in Section III, we will propose judiciously designed transceiver pairs $\{\boldsymbol{C}_{u_A}, \bar{\boldsymbol{C}}_{u_A}\}_{u_A=0}^{N_c-1}$ and $\{\boldsymbol{D}_{u_B}, \bar{\boldsymbol{D}}_{u_B}\}_{u_B=0}^{N_f-1}$, which enable separation of superimposed multiuser signals deterministically, and *regardless of* multipath propagation through frequency-selective ISI channels of maximum order L.

Based on the MU address vectors $\boldsymbol{d}_{u_B}$ defined in (10), we select the MU spreading matrices $\boldsymbol{D}_{u_B}$, and the corresponding MU separating (despreading) matrices $\bar{\boldsymbol{D}}_{u_B}$ as

$$\boldsymbol{D}_{u_B} := \boldsymbol{d}_{u_B} \otimes \boldsymbol{I}_K, \quad \bar{\boldsymbol{D}}_{u_B} := \boldsymbol{d}_{u_B} \otimes \boldsymbol{I}_{K+L}. \tag{17}$$

Using the Kronecker product definition we find that $\boldsymbol{D}_{u_B}$ and $\bar{\boldsymbol{D}}_{u_B}$ have dimensions $N_fK \times K$, and $N_f(K+L) \times (K+L)$, respectively. Recall that at this stage the spreading is performed at the frame level. The MU spreading by $\boldsymbol{D}_{u_B}$ can then be viewed as symbol-spreading followed by frame-interleaving, as shown in Fig. 5; similarly, the MU despreading by $\bar{\boldsymbol{D}}_{u_B}$ can be viewed as frame-deinterleaving followed by block-despreading.

As to the selection of the TH spreading matrices $\boldsymbol{C}_{u_A}$, and the corresponding MU separating matrices $\bar{\boldsymbol{C}}_{u_A}$, we first consider

$$\boldsymbol{c}_{u_A}^{(q)} := [c_{u_A}(qN_c), c_{u_A}(qN_c+1), \ldots, c_{u_A}(qN_c+N_c-1)]^T$$

for $q \in [0, N_f-1]$, where c_{u_A} is defined in (6), and let

$$\boldsymbol{C}_{u_A}^{(q)} := \boldsymbol{c}_{u_A}^{(q)} \otimes \boldsymbol{T}_{zp}, \quad \bar{\boldsymbol{C}}_{u_A}^{(q)} := \boldsymbol{c}_{u_A}^{(q)} \otimes \boldsymbol{I}_{K+L}$$

where $\boldsymbol{T}_{zp} := [\boldsymbol{I}_K, \boldsymbol{0}_{K\times L}]^T$ is a $(K+L)\times K$ matrix, which we term zero-padding (ZP) matrix because upon premultiplication with a $K \times 1$ vector, it appends L zeros. Based on $\boldsymbol{C}_{u_A}^{(q)}$'s and $\bar{\boldsymbol{C}}_{u_A}^{(q)}$'s, we select the $P \times N_fK$ TH spreading matrices $\boldsymbol{C}_{u_A}$, and the corresponding $P \times N_f(K+L)$ TH separating matrices $\bar{\boldsymbol{C}}_{u_A}$ as

$$\begin{aligned} \boldsymbol{C}_{u_A} &:= \operatorname{diag}\left\{\boldsymbol{C}_{u_A}^{(0)}, \boldsymbol{C}_{u_A}^{(1)}, \ldots, \boldsymbol{C}_{u_A}^{(N_f-1)}\right\} \\ \bar{\boldsymbol{C}}_{u_A} &:= \operatorname{diag}\left\{\bar{\boldsymbol{C}}_{u_A}^{(0)}, \bar{\boldsymbol{C}}_{u_A}^{(1)}, \ldots, \bar{\boldsymbol{C}}_{u_A}^{(N_f-1)}\right\}. \end{aligned} \tag{18}$$

It can be readily shown that $P = N_fN_c(K+L) = (K+L)P_c$. Recall that at this stage, the spreading is performed at the chip level. The TH spreading by $\boldsymbol{C}_{u_A}$ can then be viewed as symbol-spreading followed by chip interleaving and zero padding, as shown in Fig. 6. The properties of Kronecker products can be

used to verify the following mutual orthogonality relationships between any two users u and μ

$$\begin{aligned}
\boldsymbol{C}_{\mu_A}^{\mathcal{H}}\boldsymbol{C}_{u_A} &= \delta(\mu_A - u_A)\boldsymbol{I}_{N_fK}\\
\bar{\boldsymbol{C}}_{\mu_A}^{\mathcal{H}}\bar{\boldsymbol{C}}_{u_A} &= \delta(\mu_A - u_A)\boldsymbol{I}_{N_f(K+L)}\\
\boldsymbol{D}_{\mu_B}^{\mathcal{H}}\boldsymbol{D}_{u_B} &= N_f\delta(\mu_B - u_B)\boldsymbol{I}_K\\
\bar{\boldsymbol{D}}_{\mu_B}^{\mathcal{H}}\bar{\boldsymbol{D}}_{u_B} &= N_f\delta(\mu_B - u_B)\boldsymbol{I}_{K+L}.
\end{aligned} \tag{19}$$

Based on the (de)spreading matrix pairs in (17) and (18), we have the following observations.

Proposition 1: The $\boldsymbol{s}_{u,m}(i-1)$ dependent term in (14), that accounts for IBI, vanishes.

Proof: Recognizing that the last L rows of $\boldsymbol{C}_{u_A}$ are zeros by design, while the nonzero elements of $\boldsymbol{H}_{u,m',m,1}$ only show up in its last L columns, we have

$$\boldsymbol{H}_{u,m',m,1}\boldsymbol{C}_{u_A} = \boldsymbol{0}_{P\times N_fK} \tag{20}$$

from which it follows that $\boldsymbol{H}_{u,m',m,1}\boldsymbol{C}_{u_A}\boldsymbol{D}_{u_B}\boldsymbol{s}_{u,m}(i-1) = \boldsymbol{0}_{P\times 1}$. ∎

Furthermore, we prove in the Appendix the following.

Proposition 2: The channel matrix $\boldsymbol{H}_{u,m',m,0}$ commutes with the BS matrices $\boldsymbol{C}_{u_A}$ and $\boldsymbol{D}_{u_B}$ in (14). Specifically, it holds that $\boldsymbol{H}_{u,m',m,0}\boldsymbol{C}_{u_A}\boldsymbol{D}_{u_B}\boldsymbol{s}_{u,m}(i) = \bar{\boldsymbol{C}}_{u_A}\bar{\boldsymbol{D}}_{u_B}\check{\boldsymbol{H}}_{u,m',m}\boldsymbol{s}_{u,m}(i)$, where $\check{\boldsymbol{H}}_{u,m',m}$ is a tall Toeplitz matrix of dimension $(K+L)\times K$.

Using Propositions 1 and 2, and substituting (20) into (14), we have

$$\begin{aligned}
\boldsymbol{x}_{m'}(i) = \sum_{u_A=0}^{N_c-1}\bar{\boldsymbol{C}}_{u_A}\sum_{u_B=0}^{N_f-1}\bar{\boldsymbol{D}}_{u_B}\\
\times\sum_{m=0}^{M-1}\mathcal{P}_u\check{\boldsymbol{H}}_{u,m',m}\boldsymbol{s}_{u,m}(i) + \boldsymbol{\eta}_{m'}(i).
\end{aligned} \tag{21}$$

Based on (19) and (21), we can reexpress (15) as

$$\begin{aligned}
\boldsymbol{y}_{\mu,m'}(i) &= \bar{\boldsymbol{D}}_{\mu_B}^{\mathcal{H}}\bar{\boldsymbol{C}}_{\mu_A}^{\mathcal{H}}\sum_{u_A=0}^{N_c-1}\sum_{u_B=0}^{N_f-1}\bar{\boldsymbol{C}}_{u_A}\bar{\boldsymbol{D}}_{u_B}\\
&\quad\cdot\sum_{m=0}^{M-1}\mathcal{P}_u\check{\boldsymbol{H}}_{u,m',m}\boldsymbol{s}_{u,m}(i) + \bar{\boldsymbol{D}}_{\mu_M}^{\mathcal{H}}\bar{\boldsymbol{C}}_{\mu_A}^{\mathcal{H}}\boldsymbol{\eta}_{m'}(i)\\
&= N_f\mathcal{P}_\mu\sum_{m=0}^{M-1}\check{\boldsymbol{H}}_{\mu,m',m}\boldsymbol{s}_{\mu,m}(i) + \tilde{\boldsymbol{\eta}}_{m'}(i)
\end{aligned} \tag{22}$$

with the substitution $\tilde{\boldsymbol{\eta}}_{m'}(i) := \bar{\boldsymbol{D}}_{\mu_M}^{\mathcal{H}}\bar{\boldsymbol{C}}_{\mu_A}^{\mathcal{H}}\boldsymbol{\eta}_{m'}(i)$. Notice that the block despreading operation $\bar{\boldsymbol{D}}_{\mu_B}^{\mathcal{H}}\bar{\boldsymbol{C}}_{\mu_A}^{\mathcal{H}}$ has indeed separated the desired user μ perfectly from the MUI. Considering the $MK\times 1$ blocks $\boldsymbol{s}_\mu(i) := [\boldsymbol{s}_{\mu,0}^T(i), \boldsymbol{s}_{\mu,1}^T(i),\ldots,\boldsymbol{s}_{\mu,M-1}^T(i)]^T$, we have from (22)

$$\boldsymbol{y}_\mu(i) = N_f\mathcal{P}_\mu\check{\boldsymbol{H}}_\mu\boldsymbol{s}_\mu(i) + \tilde{\boldsymbol{\eta}}(i) \tag{23}$$

where $\boldsymbol{y}_\mu(i)$ and $\tilde{\boldsymbol{\eta}}(i)$ are $M(K+L)\times 1$ vectors generated by concatenating the output blocks from the receiver filters matched to the M waveforms, and $\check{\boldsymbol{H}}_\mu$ is the $M(K+L)\times MK$ matrix

$$\check{\boldsymbol{H}}_\mu := \begin{bmatrix}
\check{\boldsymbol{H}}_{\mu,0,0} & \check{\boldsymbol{H}}_{\mu,0,1} & \cdots & \check{\boldsymbol{H}}_{\mu,0,M-1}\\
\check{\boldsymbol{H}}_{\mu,1,0} & \check{\boldsymbol{H}}_{\mu,1,1} & \cdots & \check{\boldsymbol{H}}_{\mu,1,M-1}\\
\vdots & \vdots & \ddots & \vdots\\
\check{\boldsymbol{H}}_{\mu,M-1,0} & \check{\boldsymbol{H}}_{\mu,M-1,1} & \cdots & \check{\boldsymbol{H}}_{\mu,M-1,M-1}
\end{bmatrix}.$$

Equations (22) and (23) disclose that the superimposed received signals from multiple users can be separated deterministically, regardless of the finite-impulse response (FIR) multipath channels. This is due to the fact that the design in (17) and (18) preserves the code orthogonality among users even after *unknown* multipath propagation. Similar to [18], multipath channels with CIBS transmissions cause ISI within each symbol block, but they do not give rise to interchip interference (ICI) within the code vector; i.e., ICI is replaced by ISI. Recall that in our MS-BS-IRMA design, the BS at the first stage is accomplished by the spreading matrix $\boldsymbol{D}_{u_A}$, which is formed by symbol spreading followed by frame-interleaving; the second-stage BS is accomplished by the spreading matrix $\boldsymbol{C}_{u_B}$, which is formed by symbol spreading followed by chip interleaving and zero padding. The one-step zero padding in the second-BS stage eliminates the ICI and maintains the orthogonality among the spreading codes of both stages, namely TH and MU addresses, which in turn guarantees the deterministic multiuser separation at the receiver.

Similar to [18], we claim that the multiuser separating front-end preserves the maximum-likelihood (ML) optimality. Collecting $\bar{\boldsymbol{G}}_u := (\boldsymbol{I}_M\otimes\bar{\boldsymbol{C}}_{u_A})(\boldsymbol{I}_M\otimes\bar{\boldsymbol{D}}_{u_B})$'s to form $\bar{\boldsymbol{G}} := [\bar{\boldsymbol{G}}_0, \bar{\boldsymbol{G}}_1,\ldots,\bar{\boldsymbol{G}}_{N_u-1}]$, we obtain $\bar{\boldsymbol{G}}^{\mathcal{H}}\bar{\boldsymbol{G}} = N_f\boldsymbol{I}_{M(K+L)}$. The latter implies that if $\boldsymbol{\eta}(i)$ is white, then $\tilde{\boldsymbol{\eta}}(i)$ remains white, and

$$\Pr\left[\boldsymbol{x}(i)\,|\,\{\boldsymbol{s}_u(i)\}_{u=0}^{N_u-1}\right] = \prod_{u=0}^{N_u-1}\Pr[\boldsymbol{y}_u(i)\,|\,\boldsymbol{s}_u(i)] \tag{24}$$

where $\boldsymbol{x}(i) := [\boldsymbol{x}_0^T(i), \boldsymbol{x}_1^T(i),\ldots,\boldsymbol{x}_{M-1}^T(i)]^T$, the number of active users is $N_u = N_fN_c$ in the fully-loaded case, and Pr denotes probability; i.e., our multistage block despreading operations perform user separation (MUI elimination) without coloring the noise. Therefore, our chosen (de)spreading codes have successfully converted a MUD problem, which has to deal with both MUI and ISI in the presence of time dispersive channels, into a set of equivalent single user equalization problems without loss of optimality. In other words, if the N_u single user ISI problems in (23) are demodulated in the ML sense using, e.g., Viterbi's decoding, then computationally demanding MUD is not needed when spreading and despreading matrices are chosen as in (17) and (18).

Trading off optimality for complexity, any other equalizer can replace the ML Viterbi equalizer in decoding (23). For M-ary PPM modulation, the complexity of maximum likelihood sequence estimation (MLSE) is $\mathcal{O}(KM^{L_u})$ per symbol block of size K. The per-symbol decoding complexity is, thus, $\mathcal{O}(M^{L_u})$, irrespective of the block size K, and the maximum channel order $L = \max_u L_u$. Exploiting the finite alphabet, decision feedback equalization (DFE) can certainly be applied. Furthermore, after MUI elimination, noncoherent detection is

also possible. Striking a compromise between performance and complexity, here we consider only linear equalizers. Depending on how $\mathbf{\Gamma}_\mu$ is selected, we obtain the following linear receivers:

MF receiver

$$\mathbf{\Gamma}_\mu^{MF} := \check{\boldsymbol{H}}_\mu^{\mathcal{H}}/N_f \tag{25}$$

zero-forcing (ZF) receiver

$$\mathbf{\Gamma}_\mu^{ZF} := \left(\check{\boldsymbol{H}}_\mu^{\mathcal{H}}\check{\boldsymbol{H}}_\mu\right)^{-1}\check{\boldsymbol{H}}_\mu^{\mathcal{H}}\Big/ N_f \tag{26}$$

minimum mean-square error (MMSE) receiver

$$\mathbf{\Gamma}_\mu^{\mathrm{MMSE}} := N_f\boldsymbol{R}_\mu\check{\boldsymbol{H}}_\mu^{\mathcal{H}}\left[\boldsymbol{R}_{\tilde{\eta}} + N_f^2\check{\boldsymbol{H}}_\mu\boldsymbol{R}_\mu\check{\boldsymbol{H}}_\mu^{\mathcal{H}}\right]^{-1} \tag{27}$$

where $\boldsymbol{R}_\mu := \boldsymbol{E}\{\boldsymbol{s}_\mu(i)\boldsymbol{s}_\mu^{\mathcal{H}}(i)\}$, and $\boldsymbol{R}_{\tilde{\eta}} := \boldsymbol{E}\{\tilde{\boldsymbol{\eta}}(i)\tilde{\boldsymbol{\eta}}^{\mathcal{H}}(i)\}$.

Symbol detection is then performed based on the soft estimates $\hat{\tilde{\boldsymbol{s}}}_\mu(i)$ (cf. (16)). Defining the μth user's $K\times 1$ symbol block estimate $\hat{\boldsymbol{i}}_\mu := [\hat{I}_\mu(iK), \hat{I}_\mu(iK+1), \ldots, \hat{I}_\mu(iK+K-1)]^T$, decisions can be made according to

$$\hat{I}_\mu(iK+k) = \arg\max_m\{\hat{s}_{\mu,m}(iK+k)\}$$

for all $m \in [0, M-1],\ k \in [0, K-1]$.

So far , we have seen how MS-BS-IRMA replaces ICI with ISI and, thereby, converts a MUD problem into a set of equivalent single user equalization problems. We now look at several of its features.

A. MUI-Resilient Reception

Notice that equalization among users in MS-BS-IRMA is fully decentralized, and each user may opt to use a different equalizer, without interfering with other users. In other words, the coexistence of multiple users does not affect the performance of individual users, who are flexible to have their own channel acquisition and/or equalization choices. This is in sharp contrast with conventional IRMA systems. Let us consider the system parameters in [16], with $T_c = 2$ ns, $N_f = 512$, and $N_c = 50$. Then the maximum number of users that can be accommodated by our MS-BS-IRMA system is $N_cN_f = 25\,600$. As N_u increases in the range of $[1, 25\,600]$, no degradation in performance occurs and no additional power is required to achieve a certain BER, regardless of the multipath channel. In contrast, BER degrades in the conventional IRMA system as N_u increases, even when the channels are frequency nonselective. We will confirm this in our simulation section.

B. Rate Scalability

The capability to offer different users variable transmission rates is a very attractive feature, especially for certain multimedia applications. A thorough elaboration on the multirate capabilities of a block-spread multicarrier CDMA scheme can be found in [12]. Here we show that such services can be accommodated also within our MS-BS-IRMA system. The basic idea is to allow different users to have a different number of MU-TH address pairs $\{\boldsymbol{c}_{u_A}, \boldsymbol{d}_{u_B}\}$.

Consider assigning to the uth user a set of A_u MU-TH address pairs denoted by Ω_u. The ith transmitted information carrying block on the mth branch of user u is then given by

$$\boldsymbol{\nu}_{u,m}(i) = \sum_{\{\omega_A,\omega_B\}\in\Omega_u} \boldsymbol{C}_{\omega_A}\boldsymbol{D}_{\omega_B}\boldsymbol{s}_{u,m}^{\{\omega_A,\omega_B\}}(i) \tag{28}$$

i.e., the uth user can transmit A_u symbol blocks of length K simultaneously, each carried on a distinct MU-TH address pair $\{\omega_A, \omega_B\} \in \Omega_u$. In this way, the uth user can transmit a total number of $K_u = A_uK$ symbols during each burst of PT_c s, with a corresponding transmission rate $R_u = K_u/(PT_c)$ that is proportional to A_u for a given K and PT_c. Recall that the maximum number of mutually orthogonal MU-TH address pairs is N_cN_f, and let Ω denote the entire set of such address pairs. In order to avoid address collision and guarantee deterministic symbol block separation, two conditions have to be satisfied in the address assignment

$$\bigcup_u \Omega_u \in \Omega, \quad \forall u \in [0, N_u - 1]$$
$$\Omega_u \bigcap \Omega_\mu = \emptyset, \quad \forall u, \mu \in [0, N_u - 1], \quad \text{and } u \neq \mu$$

where $N_u \leq N_cN_f$ is the number of users. Provided each user's rate requirement, various numbers of MU-TH address pairs can be allocated accordingly to achieve multirate transmission.

C. Bandwidth Efficiency Versus Decoding Delay

From a bandwidth utilization point of view, each of the N_u users sends K information symbols every $P = N_cN_f(K+L)$ transmitted chips. Therefore, it is meaningful to define bandwidth efficiency as

$$\mathcal{E} := \frac{N_uK}{P} = \frac{N_uK}{N_cN_f(K+L)}.$$

Since in the fully loaded case, we have $N_u = N_cN_f$, it follows that:

$$\mathcal{E} := \frac{K}{K+L} \leq 1. \tag{29}$$

For a fixed L, larger K implies higher bandwidth efficiency. But as K increases, the decoding latency increases as well, because the receiver needs to wait for the entire P-long block before decoding symbols in the block.

V. Simulated Performance

In our simulations, two channel models are employed. In the first one, the channel has 400 paths equally spaced in time within the maximum delay spread. The path amplitudes are modeled as Gaussian variables, and they are linearly weighted with weights decreasing to zero at the maximum delay spread. The second-channel model is generated according to [4], [9], where rays arrive in several clusters within an observation window. The cluster arrival times are modeled as Poisson variables with cluster arrival rate Λ. Rays within each cluster also arrive according to a Poisson process with ray arrival rate λ. The amplitude of each arriving ray is a Rayleigh distributed random variable having exponentially decaying mean-square value with parameters Γ and γ. Parameters of this channel model are chosen as: $\Gamma = 33$ ns, $\gamma = 5$ ns, $1/\Lambda = 2$ ns, and $1/\lambda = 0.5$ ns.

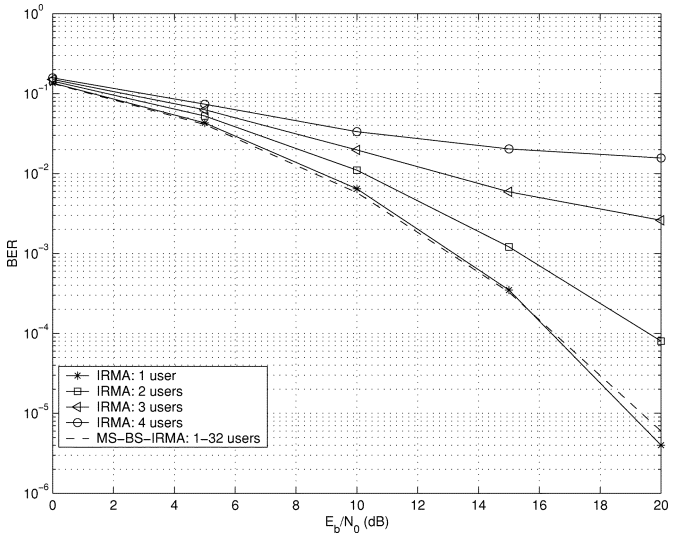

Fig. 7. Comparing BER performance of a conventional IRMA system with a MS-BS-IRMA system as the number of active users increases (channel model 1).

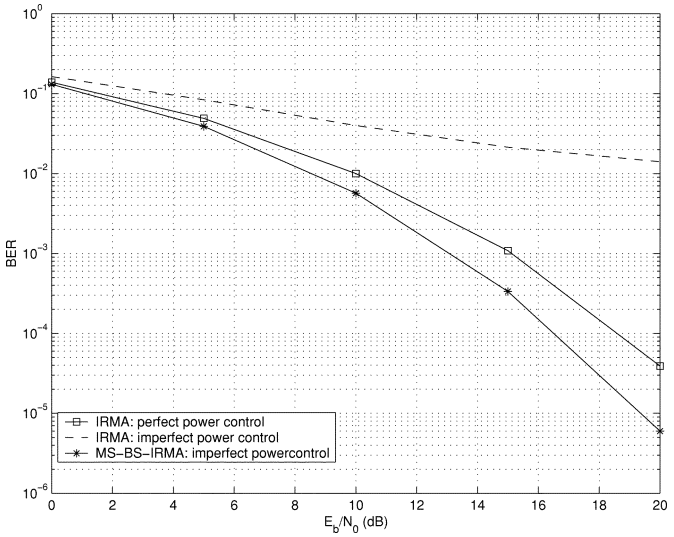

Fig. 8. Comparing BER performance of conventional IRMA against MS-BS-IRMA with imperfect power control (two active users-channel model 1).

We select the pulse shaper to be the second derivative of the Gaussian function $w(t) = \sqrt{\tau^3/3}(2/\pi)^{1/4}\exp(-t^2/\tau^2)$, which has been normalized to have unit energy. The parameter τ is chosen to be 0.1225 ns to obtain a pulsewidth of 0.7 ns. The system parameters are as follows: constellation size $M = 2$, which corresponds to a binary modulation, with every symbol transmitted repeatedly over $N_f = 8$ frames, and each frame composed of $N_c = 4$ chips. As in [16], we have chosen the frame duration $T_f = 100$ ns, which is also the maximum delay spread.

Test A: First, we test the performance of MF (RAKE) receiver of a conventional IRMA system against our MS-BS-IRMA system in the presence of frequency-selective channels. In the conventional IRMA system, a filter matched to the desired user's TH code is used. We confine the number of users in the conventional IRMA system $N_u \leq N_c$, so that orthogonal TH codes can be employed to avoid collision. For both systems, we assume that adjacent symbols of a specific user are placed far apart to avoid ISI, and symbol-by-symbol reception is performed at the receiver.

Case 1: Uplink scenario with perfect power control (or equivalently downlink scenario), i.e., $\mathcal{P}_u = 1, \forall u$, is considered. The number of users in the conventional IRMA system is increased from one up to four. Because MUI is eliminated deterministically, our proposed system exhibits performance that remains invariant as the number of active users changes in the range of $1 \leq N_u \leq 32$. While in the conventional IRMA system, as the number of active users increases, the BER performance degrades accordingly. Notice that although the employment of orthogonal TH codes avoids collision in the conventional IRMA system, the MUI induced by multipath propagation affects the system performance considerably. Fig. 7 shows the ensemble performance over 1 000 channel realizations.

Case 2: Uplink scenario with imperfect power control is considered here. The number of active users for both systems is set to be two, with user 1 being the desired user. Supposing that the effective transmission power of user 2 is twice that of user 1 due to near–far effect, we compare the BER performance of the two systems. Thanks to the deterministic multiuser separation performed at the front-end of our proposed receiver, the imperfect power control has no effect on the BER performance. In contrast, the conventional IRMA system encounters degradation due to this phenomenon. The ensemble performance over 1 000 channel realizations is shown in Fig. 8.

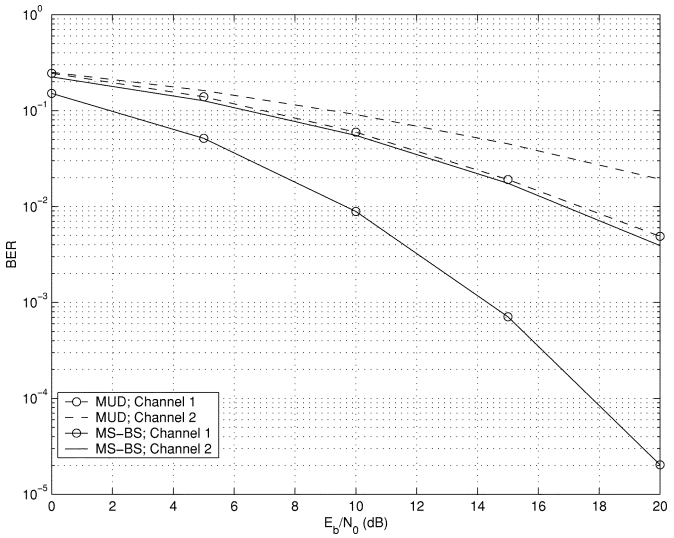

Fig. 9. BER versus E_b/N_0 for ZF receiver with binary symbols and $N_f = 8$, $N_c = 4$. Block size $K = 2$. Number of active users in MUD-IRMA system: 4. Number of active users in MS-BS-IRMA system: 32.

Test B: To further illustrate the performance of the proposed IRMA scheme, we simulate both the novel MUI-free MS-BS-IRMA, and the MUD-IRMA in [5] and [6]. Recall that our proposed model applies to both uplink and downlink scenario, while the latter applies only to downlink. The aforementioned system parameters allow for maximum $N_u = N_c N_f = 32$ users in the MS-BS-IRMA system, and $N_u = N_c = 4$ in the MUD-IRMA system. The block size is chosen to be $K = 2$.

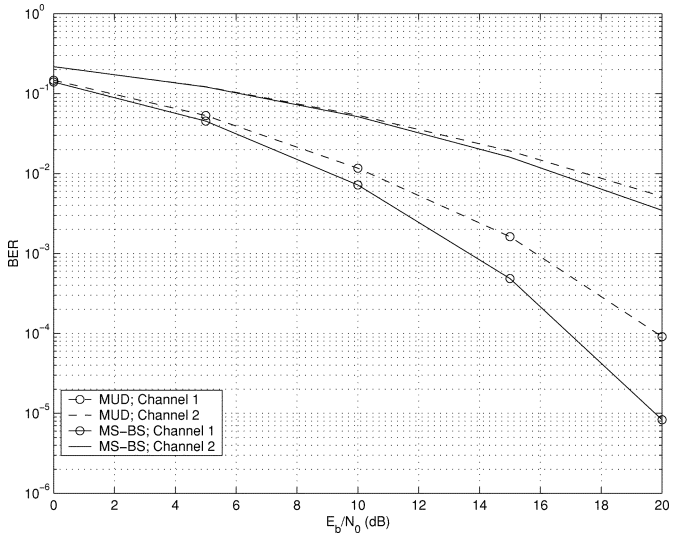

Fig. 10. BER versus E_b/N_0 for MMSE receiver with binary symbols and $N_f = 8$, $N_c = 4$. Block size $K = 2$. Number of active users in MUD-IRMA system: 4. Number of active users in MS-BS-IRMA system: 32.

Figs. 9 and 10 depict the ensemble BER performance over 1 000 channel realizations for the ZF and MMSE linear receivers based on the two digital IRMA schemes, namely MUD-IRMA and MS-BS-IRMA. In all cases, the MMSE receivers provide better performance. For all receivers and both channel models, the MS-BS receivers consistently outperform their MUD counterparts, while accommodating much more users.

VI. Conclusion

A novel MUI-resilient digital IRMA system was developed in this paper for uplink or downlink transmissions over ISI multipath channels. Relying on MS-BS, a MUD problem was converted into a set of equivalent single-user equalization problems. The performance of individual users neither depends on the number of users in the system, nor on the power of other users. As a result, our proposed system is capable of supporting a large number of ultra-wideband users communicating over frequency-selective multipath environments.

Appendix
Proof of Proposition 2

Let $\tilde{\boldsymbol{H}}_{u,m',m,0}$ be the $N_c(K+L) \times N_c(K+L)$ lower triangular Toeplitz matrix with first column $[h_{u,m',m}(0), h_{u,m',m}(1), \ldots, h_{u,m',m}(L), 0, \ldots, 0]^T$, and $\tilde{\boldsymbol{H}}_{u,m',m,1}$ be the $N_c(K+L) \times N_c(K+L)$ upper triangular Toeplitz matrix with first row $[0, \ldots, 0, h_{u,m',m}(L), h_{u,m',m}(L-1), \ldots, h_{u,m',m}(1)]$. The $P \times P$ matrix $\boldsymbol{H}_{u,m',m,0}$ in (14) can be split into smaller blocks as

$$\boldsymbol{H}_{u,m',m,0} = \boldsymbol{I}_{N_f} \otimes \tilde{\boldsymbol{H}}_{u,m',m,0} + \boldsymbol{J}_{N_f} \otimes \tilde{\boldsymbol{H}}_{u,m',m,1} \quad (30)$$

where $\boldsymbol{I}_{N_f}$ is the $N_f \times N_f$ identity matrix, and $\boldsymbol{J}_{N_f}$ is the $N_f \times N_f$ shifting matrix with first column $[0, 1, 0, \ldots, 0]^T$. For the same reason that results in (20), we have $\tilde{\boldsymbol{H}}_{u,m',m,1}\boldsymbol{C}_{u_A}^{(q)} = \boldsymbol{0}_{N_c(K+L)\times K}$, $\forall q \in [0, N_f - 1]$. It follows that:

$$\begin{aligned}\left(\boldsymbol{J}_{N_f} \otimes \tilde{\boldsymbol{H}}_{u,m',m,1}\right)\boldsymbol{C}_{u_A} &= \left(\boldsymbol{J}_{N_f} \otimes \tilde{\boldsymbol{H}}_{u,m',m,1}\right)\operatorname{diag}\left\{\boldsymbol{C}_{u_A}^{(0)}, \ldots, \boldsymbol{C}_{u_A}^{(N_f-1)}\right\} \\ &= \boldsymbol{0}_{P\times N_f K}\end{aligned}$$

and

$$\begin{aligned}\boldsymbol{H}_{u,m',m,0}\boldsymbol{C}_{u_A} &= (\boldsymbol{I}_{N_f} \otimes \tilde{\boldsymbol{H}}_{u,m',m,0})\boldsymbol{C}_{u_A} \\ &= \operatorname{diag}\left\{\tilde{\boldsymbol{H}}_{u,m',m,0}\boldsymbol{C}_{u_A}^{(0)}, \ldots, \tilde{\boldsymbol{H}}_{u,m',m,0}\boldsymbol{C}_{u_A}^{(N_f-1)}\right\}. \quad (31)\end{aligned}$$

In a manner similar to (30), $\tilde{\boldsymbol{H}}_{u,m',m,0}$ can be further split into blocks of dimension $(K+L)\times(K+L)$ as

$$\tilde{\boldsymbol{H}}_{u,m',m,0} = \boldsymbol{I}_{N_c} \otimes \bar{\boldsymbol{H}}_{u,m',m,0} + \boldsymbol{J}_{N_c} \otimes \bar{\boldsymbol{H}}_{u,m',m,1} \quad (32)$$

where $\bar{\boldsymbol{H}}_{u,m',m,0}$ and $\bar{\boldsymbol{H}}_{u,m',m,1}$ are upper and lower triangular Toeplitz matrices defined accordingly. Making use of Kronecker product properties, we have

$$\begin{aligned}\tilde{\boldsymbol{H}}_{u,m',m,0}\boldsymbol{C}_{u_A}^{(q)} &= \left(\boldsymbol{I}_{N_c} \otimes \bar{\boldsymbol{H}}_{u,m',m,0}\right)\left(\boldsymbol{c}_{u_A}^{(q)} \otimes \boldsymbol{T}_{zp}\right) \\ &\quad + \left(\boldsymbol{J}_{N_c} \otimes \bar{\boldsymbol{H}}_{u,m',m,1}\right)\left(\boldsymbol{c}_{u_A}^{(q)} \otimes \boldsymbol{T}_{zp}\right) \\ &= \boldsymbol{c}_{u_A}^{(q)} \otimes (\bar{\boldsymbol{H}}_{u,m',m,0}\boldsymbol{T}_{zp}) \\ &= \left(\boldsymbol{c}_{u_A}^{(q)} \otimes \boldsymbol{I}_{K+L}\right)(\bar{\boldsymbol{H}}_{u,m',m,0}\boldsymbol{T}_{zp}) \\ &= \bar{\boldsymbol{C}}_{u_A}^{(q)}\check{\boldsymbol{H}}_{u,m',m} \quad (33)\end{aligned}$$

with $\check{\boldsymbol{H}}_{u,m',m} := \bar{\boldsymbol{H}}_{u,m',m,0}\boldsymbol{T}_{zp}$ a tall Toeplitz matrix of dimension $(K+L)\times K$. Substituting (33) into (31), we have

$$\begin{aligned}\boldsymbol{H}_{u,m',m,0}\boldsymbol{C}_{u_A} &= \operatorname{diag}\left\{\bar{\boldsymbol{C}}_{u_A}^{(0)}\check{\boldsymbol{H}}_{u,m',m}, \ldots, \bar{\boldsymbol{C}}_{u_A}^{(N_f-1)}\check{\boldsymbol{H}}_{u,m',m}\right\} \\ &= \bar{\boldsymbol{C}}_{u_A}\left(\boldsymbol{I}_{N_f} \otimes \check{\boldsymbol{H}}_{u,m',m}\right).\end{aligned}$$

Furthermore, noticing that

$$\begin{aligned}\left(\boldsymbol{I}_{N_f} \otimes \check{\boldsymbol{H}}_{u,m',m}\right)\boldsymbol{D}_{u_B} &= \left(\boldsymbol{I}_{N_f} \otimes \check{\boldsymbol{H}}_{u,m',m}\right)(\boldsymbol{d}_{u_B} \otimes \boldsymbol{I}_K) \\ &= \boldsymbol{d}_{u_B} \otimes \check{\boldsymbol{H}}_{u,m',m} \\ &= (\boldsymbol{d}_{u_B} \otimes \boldsymbol{I}_{K+L})\check{\boldsymbol{H}}_{u,m',m} \\ &= \bar{\boldsymbol{D}}_{u_B}\check{\boldsymbol{H}}_{u,m',m}\end{aligned}$$

we have

$$\boldsymbol{H}_{u,m',m,0}\boldsymbol{C}_{u_A}\boldsymbol{D}_{u_B} = \bar{\boldsymbol{C}}_{u_A}\bar{\boldsymbol{D}}_{u_B}\check{\boldsymbol{H}}_{u,m',m}. \quad (34)$$

References

[1] J. R. Foerster, "The effects of multipath interference on the performance of UWB systems in an indoor wireless channel," in *Proc. Vehicular Technology Conf.*, vol. 2, Rhodes Island, Greece, 2001, pp. 1176–1180.

[2] G. B. Giannakis, Z. Wang, A. Scaglione, and S. Barbarossa, "AMOUR-generalized multicarrier transceivers for blind CDMA regardless of multipath," *IEEE Trans. Commun.*, vol. 48, pp. 2064–2076, Dec. 2000.

[3] S. S. Kolenchery, J. K. Townsend, and J. A. Freebersyser, "A novel impulse radio network for tactical wireless communications," in *Proc. Milcom Conf.*, Bedford, MA, Oct. 1998, pp. 59–65.

[4] H. Lee, B. Han, Y. Shin, and S. Im, "Multipath characteristics of impulse radio channels," in *Proc. Vehicular Technology Conf.*, Tokyo, Japan, 2000, pp. 2487–2491.

[5] C. J. Le Martret and G. B. Giannakis, "All-digital impulse radio with multiuser detection for wireless cellular systems," *IEEE Trans. Communications*, vol. 50, pp. 1440–1450, Sept. 2002.

[6] C. J. Le Martret and G. B. Giannakis, "All-digital PPM Impulse Radio for multiple-access through frequency-selective multipath," in *Proc. Sensor Array Multichannel Signal Processing Workshop*, Boston, MA, Mar. 2002, pp. 22–26.
[7] F. Ramirez-Mireles and R. A. Scholtz, "Multiple access with time-hopping and block waveform PPM modulation," in *Proc. Int. Conf. Commun.*, vol. 2, Toronto, ON, Canada, 1998, pp. 775–779.
[8] ——, "System performance analysis of impulse radio modulation," in *Proc. Radio Wireless Conf.*, Colorado Springs, CO, Aug. 1998, pp. 67–70.
[9] A. A. M. Saleh and R. A. Valenzuela, "A statistical model for indoor multipath propagation," *IEEE J. Select. Areas Commun.*, vol. JSAC-5, pp. 128–137, Feb. 1987.
[10] R. A. Scholtz, "Multiple access with time-hopping impulse modulation," in *Proc. Milcom Conf.*, Boston, MA, Oct. 1993, pp. 447–450.
[11] Z. Wang and G. B. Giannakis, "Wireless multicarrier communications: Where Fourier meets Shannon," *IEEE Signal Processing Mag.*, vol. 17, pp. 29–48, May 2000.
[12] ——, "Block precoding for MUI/ISI-resilient generalized multicarrier CDMA with multirate capabilities," *IEEE Trans. Commun.*, vol. 49, pp. 2016–2027, Nov. 2001.
[13] M. Z. Win and Z. A. Kostic, "Virtual path analysis of selective Rake receiver in dense multipath channels," *IEEE Commun. Lett.*, vol. 3, pp. 308–310, Nov. 1999.
[14] M. Z. Win and R. A. Scholtz, "Impulse radio: How it works," *IEEE Commun. Lett.*, vol. 2, pp. 36–38, Feb. 1998.
[15] ——, "On the robustness of ultra-wide bandwidth signals in dense multipath environments," *IEEE Commun. Lett.*, vol. 2, pp. 51–53, Feb. 1998.
[16] ——, "Ultra-wide bandwidth time-hopping spread-spectrum impulse radio for wireless multiple-access communications," *IEEE Trans. Commun.*, vol. 48, pp. 679–691, Apr. 2000.
[17] P. II. Withington and L. W. Fullerton, "An impulse radio communications system," in *Proc. Int. Conf. Ultra-Wideband, Short-Pulse Electromagnetics*, Brooklyn, NY, Oct. 1992, pp. 113–120.
[18] S. Zhou, G. B. Giannakis, and C. Le Martret, "Chip-interleaved block-spread code division multiple access," *IEEE Trans. Commun.*, vol. 50, pp. 235–248, Feb. 2002.

Liuqing Yang (S'02) received the B.S. degree in electronics engineering from the Huazhong University of Science and Technology, Wuhan, China, in 1994, and the M.Sc. degree in electrical engineering from the University of Minnesota, Minneapolis, in 2002, where she is currently working toward the Ph.D. degree in the the Department of Electrical and Computer Engineering.

Her current interests include the channel and timing acquisition, multiuser detection, space–time coding, and networking aspects of ultra-wideband communication systems.

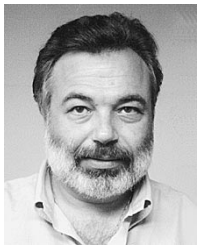

Georgios B. Giannakis (S'84–M'86–SM'91–F'97) received the Diploma in electrical engineering, in 1981 from the National Technical University of Athens, Greece, the M.Sc. degree in electrical engineering in 1983, the M.Sc. degree in mathematics in 1986, and the Ph.D. degree in electrical engineering, in 1986, all from the University of Southern California (USC), Los Angeles.

After lecturing for one year at USC, he joined the University of Virginia, Charlotesville, in 1987, where he became a Professor of electrical engineering in 1997. Since 1999, he has been a Professor in the Department of Electrical and Computer Engineering, University of Minnesota, Minneapolis, where he now holds an ADC Chair in Wireless Telecommunications. His general interests span the areas of communications and signal processing, estimation and detection theory, time-series analysis, and system identification—subjects on which he has published more than 150 journal papers, 290 conference papers, and two edited books. His current research topics focus on transmitter and receiver diversity techniques for single and multiuser fading communication channels, precoding and space–time coding for block transmissions, multicarrier, and ultra-wideband wireless communication systems. He is a frequent consultant for the telecommunications industry.

Dr. Giannakis is the (co-) recipient of four Best Paper Awards from the IEEE Signal Processing Society (1992, 1998, 2000, and 2001). He also received the Society's Technical Achievement Award in 2000. He co-organized three IEEE Signal Processing Workshops, and Guest Edited (co-edited) four special issues. He has served as Editor in Chief for the IEEE SIGNAL PROCESSING LETTERS, Associate Editor for the IEEE TRANSACTIONS ON SIGNAL PROCESSING, and the IEEE SIGNAL PROCESSING LETTERS, Secretary of the Signal Processing Conference Board, Member of the Signal Processing Publications Board, Member and Vice-Chair of the Statistical Signal and Array Processing Technical Committee, and Chair of the Signal Processing for Communications Technical Committee. He is a Member of the Editorial Board for the PROCEEDINGS OF THE IEEE, and the Steering Committee of the IEEE TRANSACTIONS ON WIRELESS COMMUNICATIONS. He is a Member of the IEEE Fellows Election Committee, the IEEE Signal Processing Society's Board of Governors.